Cambridge Centre for Computational Chemical Engineering

University of Cambridge

Department of Chemical Engineering

Preprint ISSN 1473 – 4273

Multivariate Soot Particle Models

Matthew S Celnik [1] , Abhijeet Raj [1] , Sebastian Mosbach [1] ,

Richard H West [1] , Markus Kraft [1] *

released: 2 July 2008

[1] Department of Chemical Engineering
University of Cambridge
New Museums Site
Pembroke Street
Cambridge, CB2 3RA
UK
E-mail: mk306@cam.ac.uk

Preprint No. 60

c4e

Key words and phrases: modelling, multivariate, soot, engine, stochastic, KMC, aromatic

Edited by
Cambridge Centre for Computational Chemical Engineering
Department of Chemical Engineering
University of Cambridge
Cambridge CB2 3RA
United Kingdom.

Fax: + 44 (0)1223 334796
E-Mail: c4e@cheng.cam.ac.uk
World Wide Web: http://www.cheng.cam.ac.uk/c4e/

Abstract

This paper presents a detailed model for soot which takes the chemical and structural properties of an individual particle into account. The model is applied to laboratory flames as well as to an internal combustion engine. An aromatic site model for soot particles is presented which incorporates detailed chemical information about a soot particle's reactive sites into the computationally efficient site-counting model. A primary-particle aggregate model is presented which accounts for the fractal structure of soot particles. By approximating the collision steps of aggregate formation, 3D structural representation of soot particles can be generated for different pressure regimes, although only the free-molecular regime is considered here. An algorithm for such 3D particle structure generation is presented for the specific application of generating TEM-style images as a diagnostic tool. The Aromatic Site Counting - Primary Particle (ARS-SC-PP) model is used to simulate soot formation in a laminar premixed flame and in an internal combustion engine. The latter being achieved by incorporating the detailed soot model into the stochastic reactor model, previously used for engine simulations.

Contents

1 Introduction

Soot particle growth models in the past have been very simple. This was in part due to the limitations of the numerical methods used, such as moment methods [12], sectional methods [31, 35] and Galerkin methods [3]. These are efficient algorithms, but their complexity and computational expense scale approximately exponentially with the size of the particle type space. Monte Carlo methods [6], however, can be easily scaled to model very complex particles [5, 9, 25]. This paper shall focus on the implementation of complex multivariate particle models using Monte Carlo techniques.

In order to fully characterise soot particles a description of both the particle structure and the particle chemistry must be developed. Many current soot models are based on the work of Frenklach and Wang [14]. In that model soot growth occurs through the addition of acetylene (C_2H_2) by processes analogous to those for small PAHs. Only one acetylene addition process was defined by Appel et al. [2], though a more complete set of processes has been presented since [9, 15].

A large amount of work has been conducted into the shape and structure of soot particles. There is experimental evidence that soot particles consist of fractal-like structures [23], hence structure models of increasing complexity have been developed using this assumption. Surface-volume and fractal particle descriptions [21, 29] have been used which describe particles by two coordinates, typically a volume and a shape parameter or surface area. Full 3D aggregate particle representations have also been used [4, 25]. A lot of work has been completed to study the chemical nature of single particles [11, 15, 33, 34]. Frenklach [11] developed a detailed mechanistic model of PAH surface growth, which has been used to simulate the growth of PAH surfaces [13, 15]. Violi [33] used kinetic Monte Carlo — molecular dynamics (KMC-MD) to simulate the growth of 3D PAH structures. Violi and Izvekov [34] also attempted to model the aggregate structure of soot particles using these PAH structures by considering their interaction.

In this paper a combined soot surface chemistry and primary particle model is presented which builds on the soot model of Frenklach and Wang [14] by describing soot particles by their aromatic structure. This model combines models presented elsewhere by Celnik et al. [9] and West et al. [36]. The model is then used to simulate a premixed flame and an internal combustion engine.

2 Aromatic-site model

The model reviewed in this section has previously been published by Celnik et al. [9]. A description of PAH surface sites was developed in order to identify a suitable data structure for the population balance model. This description was based on the following observable rules:

1. PAHs can be described by the number of surface "sites". For filled PAHs these sites will form a closed loop around the PAH edge.
2. Each surface carbon belongs to two "sites".

3. Each site consists of two surface carbon atoms (those available for reaction).
4. The previous points require that each site has two neighbouring sites.
5. A site can be distinguished by the total number of carbon atoms it contains. Acceptable counts are 2, 3, 4 and 5 carbon atoms.
6. Surface processes affect the reacting site and at least its two neighbouring sites.

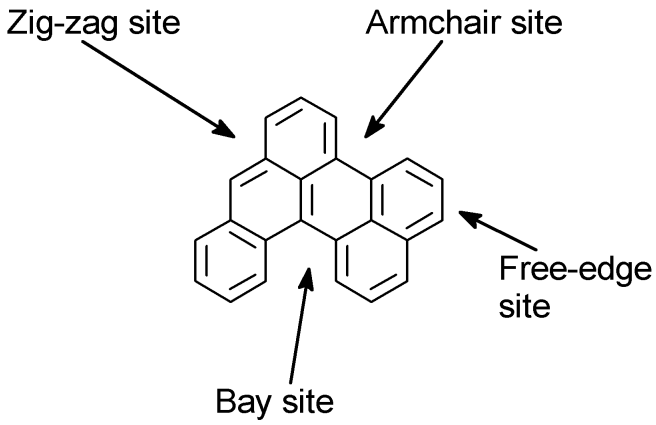

Figure 1: *An example PAH structure showing all the different principal site types.*

In this nomenclature a surface carbon is one available for reaction which has a bonded H atom. Bulk carbon shall describe carbons in the graphene lattice. Figure 1 gives the nomenclature for different site types. A site with two carbon atoms is called a "free-edge" (ED), a site with three carbon atoms is called a "zig-zag" (ZZ) [11] , a site with four carbon atoms is called an "armchair" (AC) [15] (also called elsewhere a "boat" site [11]) and a site with five carbon atoms shall be called a "bay" (BY). In general the addition of a ring *beside* any site increases its carbon count by one, thereby converting it into a different site. Similarly the removal of a ring will decrease the carbon count of a site by one. The exception to these rules is the addition of a ring beside a bay. Clearly adding an additional carbon to a bay generates a new ring, which in turns affects the next neighbouring site of the bay. A model for 5-member ring addition and conversion to 6-member rings is included in this study similar to that presented by Frenklach et al. [15], however, 5-member rings are not modelled as part of the PAH graphitic lattice. In this nomenclature R5 denotes a 5-member ring on a zig-zag site. A zig-zag site cannot react further once occupied by a 5-member ring.

3 Surface processes

Only hydrogen-abstraction carbon-addition (HACA) processes, analogous to those for small PAHs, are considered here. These processes essentially proceed via the creation

of surface radical sites by hydrogen abstraction, followed by the addition of acetylene to those sites. This mechanism for soot formation has been studied extensively since the early 1990s [14], and many variations on the theme have been discussed. The processes are discussed and listed by Celnik et al. [9]. The rate expressions for these jump processes have been obtained by assuming intermediate species to be in steady-state [9] and that the ring addition and desorption steps are irreversible. The jump processes are summarised in table 1.

It is important to note that some of the processes listed in table 1 are dependent on two sites occurring consecutively in the PAH edge. These are termed combined-sites here.

4 Site-counting model

It is the goal of this work to developed a detailed chemical and physical model of soot particles which can be solved in acceptable computation times for whole ensembles of particles. This requires the aromatic structure of PAHs and soot particles to be formally defined in a computational context. Here the fundamental state space is described, which is the minimum sufficient to fully describe a planar PAH molecule. From this state space progressively simpler data structures can be defined to enable efficient computation, while retaining most of the fundamental information. The site-counting model is formulated under the assumption that soot particles are formed primarily of stacked planar PAHs. It is anticipated that 3D structures do exist and that the addition of aliphatic chemical species may also play an important role in soot formation, however, these have been neglected for the present model. In principal the concepts of the site-counting model should allow these assumptions to be relaxed in future.

4.1 Fundamental particle state space

The structure of a PAH is defined by the position of the C atoms and the bonds between them. The similarity between the structures of PAHs and graphite ensures that a C atom can form bonds with a maximum of three other C or H atoms. It is possible to determine the structure of a PAH molecule if the information about the position of a carbon atom and the relative positions of the surrounding C atoms bonded to it are known. Therefore, the simplest state space E required to track the structure of a planar PAH molecule can be given by:

$$E = (i,\ j,\ i_1,\ j_1,\ i_2,\ j_2,\ i_3,\ j_3) \in \mathbb{Z}^8 \tag{1}$$

where $(i,\ j)$ are the coordinates of a C atom, and $(i_n,\ j_n)_{n=1,\ 2,\ 3}$ are the coordinates of the C atoms bonded to the C atom at $(i,\ j)$. The further generalisation of this state space to 3D is possible by including an additional coordinate and defining them in the set of real numbers.

While this state space is sufficient to fully define a PAH structure, definition of the Monte-Carlo jump processes on it is very difficult. Higher order data structures are required.

Table 1: *Jump processes. The reaction steps and the rate constants have been obtained from Celnik et al. [9], Frenklach et al. [15]. The activation energies are in units of kcal/mol.*

Reaction	Site	Jump process	Rate constant, k
(1) Free-edge growth	FE	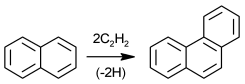	$1.1 \times 10^7 T^{1.71} e^{\frac{-3.9}{RT}}$
(2) R6 desorption	R6	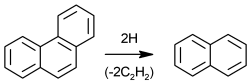	$1.3 \times 10^{11} T^{1.08} e^{\frac{-70.42}{RT}}$
(3) R5 addition	ZZ	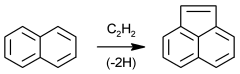	$6.8 \times 10^{11} e^{\frac{-22}{RT}}$
(4) R5 desorption	R5	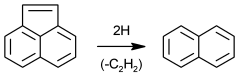	$1.6 \times 10^{14} e^{\frac{-42.42}{RT}}$
(5) Armchair growth	AC	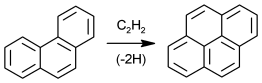	$8 \times 10^7 T^{1.56} e^{\frac{-3.8}{RT}}$
(6) 5- to 6-member ring conversion at free-edge	R5FE	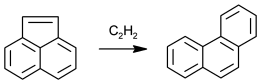	$1.1 \times 10^7 T^{1.71} e^{\frac{-3.9}{RT}}$
(7) 6- to 5-member ring conversion	R6_AC	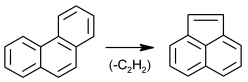	$1.3 \times 10^{11} T^{1.08} e^{\frac{-70.42}{RT}}$
(8) 5- to 6-member ring conversion at armchair	R5AC	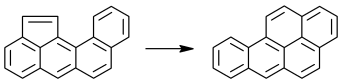	1.34×10^{12}
(9) R6 oxidation by O_2	R6	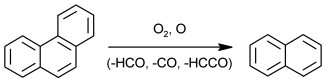	$9.7 \times 10^3 T^{2.42} e^{\frac{-38.48}{RT}}$
(10) R6 oxidation by OH	R6	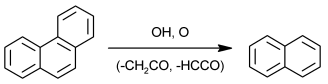	$2.2 \times 10^{12} e^{\frac{-31.4}{RT}}$
(11) AC oxidation by O_2	FE	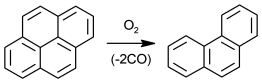	$9.7 \times 10^3 T^{2.42} e^{\frac{-38.48}{RT}}$
(12) AC oxidation by OH	FE	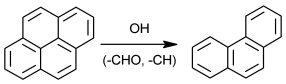	$2.2 \times 10^{12} e^{\frac{-31.4}{RT}}$
(13) R5 shift	R5ZZ	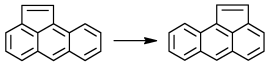	1.34×10^{12}

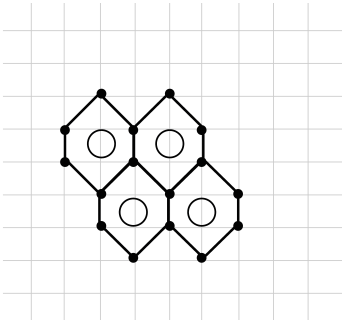

Figure 2: *An example grid showing a pyrene molecule.*

4.2 Kinetic-Monte Carlo data structure

A 2D kinetic-Monte Carlo data structure can be defined for planar PAH molecules by placing the molecule on a 2D grid, such as that in figure 2. This grid neglects the true bond lengths, which is acceptable as the bonds are implicitly represented in the rate expressions by the surface sites.

In order to make the definition of jump processes easier using the above defined state space, two vectors are defined: a carbon atom vector c, and a site vector s. The vector c stores the following information: the two site types of which the C atom is a part, S_1 and S_2, the site indices (each site of a particular type is differentiated from others based on its index), S_{in_1} and S_{in_2}, the carbon atom type (bulk or surface), C_{type}, and its spatial coordinates, i and j. Thus, c can be represented as:

$$c = (S_1,\ S_2,\ S_{in_1},\ S_{in_2},\ C_{type},\ i,\ j) \in \mathbb{Z}^7$$

A site vector s stores the following information: site type, S_{type}, site index (explained above), S_{in}, and the coordinates of the two surface C atoms, $(i_1,\ j_1)$ and $(i_2,\ j_2)$. Therefore, s can be represented as:

$$s = (S_{type},\ S_{in},\ i_1,\ j_1,\ i_2,\ j_2) \in \mathbb{Z}^6$$

4.2.1 Typical KMC-ARS result

A typical PAH structure generated using the KMC-ARS model is shown in figure 3. This molecule was generated after 3 ms in a C_2H_2 flame at 2.67 kPa, and with a C/O ratio of 0.8.

4.3 Site-counting data structure

The above KMC data structure is still too complex to be applied to an ensemble of particles, given that each particle would consist of many PAH molecules. The site-counting

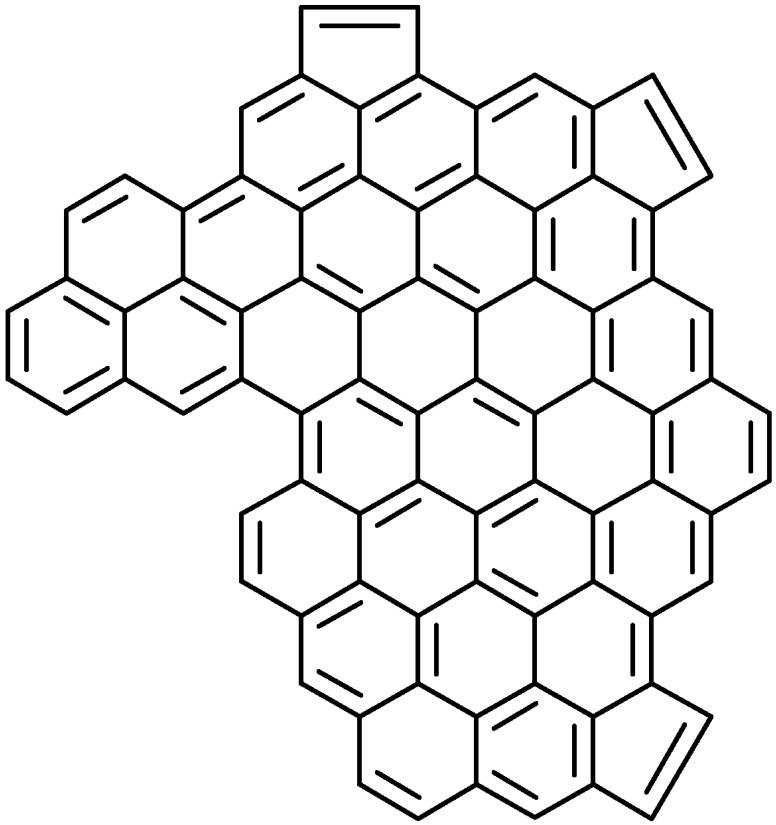

Figure 3: *A typical PAH molecule generated using the KMC-ARS model. C_2H_2 flame conditions were 2.67 kPa pressure a C/O ratio of 0.8. This molecule was generated after 3 ms of flow time.*

model has been developed to describe the aromatic structure of soot particles by nine variables only. Hence particles are described by a 9-dimensional type X_{sc}:

$$X_{sc} = (C, H, N_{ed}, N_{zz}, N_{ac}, N_{bay}, N_{R5}, S_a, N_{PAH})$$

where N_x is the number of site type x, C and H are the number of carbon and hydrogen atoms respectively, S_a is the surface area of the particle and N_{PAH} is the number of PAHs which make up the particle. By tracking the number of sites, but neglecting their relative positions this data structure allows complete particle systems to be simulated quickly.

Each process listed in table 1 must change the particle state space in a clearly defined way. The state space changes were formulated by consideration of the underlying physical processes and consideration of PAH sites discussed earlier. The particle state changes are given in table 2. Note that the R5 shift process has no effect in the site-counting model, therefore it is neglected from this table.

When a ring is added or desorbed from a PAH site it necessarily changes the structure of the PAH surface. Each site has two neighbouring sites, which must both be updated. In general, ring addition increases the number of carbon atoms in the neighbouring sites by one each (incrementing), and ring desorption decreases the number of carbon atoms by one each (decrementing). This change to the neighbouring site types occurs according to the rules in table 3.

4.4 Equation closure

For particles of type x, the site counting model can be expressed as an ODE of the form:

$$\frac{dx}{dt} = F\left(x, N_{R6\_AC}, N_{R5FE}, N_{R5AC}, N_{R5ZZ}, N_{R6}, b_{ij}\right) \tag{2}$$

where N_y is the number of combined-site type y in the particle, b_{ij} is the number of site type j next to site type i and $i, j \in (ED, ZZ, AC, BY, R5)$. The form of the right-hand side function F is defined by the jump processes, the inception processes and the coagulation process. It is clear that the above equation is not closed, as expressions for N_{R6_AC}, N_{R5FE}, N_{R5AC}, N_{R5ZZ}, N_{R6} and the b_{ij} values are required. In the previous work [8, 9] estimates of the combined-site concentrations were found using linear correlations, obtained from the KMC-ARs model, with a single known quantity. These correlations are discussed in a subsequent section.

The linear correlations were developed by simulating the 2D structural evolution of a few PAH molecules in a fixed chemical environment at different temperatures in the range 1500 K to 2000 K using a KMC code. While such correlations may not be ideal, statistical studies of PAH structures are essentially non-existent, so they should give a reasonable first approximation. It is intended to perform an in-depth study on this topic at a future point.

Not all site configurations are equally likely, hence not all sites are equally probable to be neighbours of a reacting site. In order to correctly select neighbouring sites a further

Table 2: *Changes to particle state due to jump processes in table 1* [a]

Process		C	H	N_{ed}	N_{zz}	N_{ac}	N_{bay}	N_{R5}	N_{PAH}	Inc.[2]	Dec.[3]
Inception Processes											
	Pyrene inception	32	20	12	8	0	0	0	2	.	.
Surface Processes											
S1	Free-edge ring growth	+4	+2	+2	.	.	.	.	.	2	.
S2	Free-edge ring desorption	-4	-2	-2	.	.	.	.	.	.	2
S3	R5 addition	+2	.	.	-1	.	.	+1	.	.	.
S4	R5 desorption	-2	.	.	+1	.	.	-1	.	.	.
S5	Armchair ring growth	+2	.	+1	.	-1	.	.	.	2	.
S6	R5-R6 conversion at free-edge	+2	+2	+2	.	+1	.	-1	.	1	.
S7	R6-R5 conversion at free-edge	-2	-2	-2	.	-1	.	+1	.	.	1
S8	R5-R6 conversion at armchair	.	.	+1	.	.	.	-1	.	1	.
PAH Condensation Processes											
	Pyrene condensation	+16	+10	+6	+4	.	.	.	+1	.	.
Oxidation Processes											
S9	Free-edge O_2 oxidation	-4	-2	-2	.	.	.	.	.	.	2
S10	Free-edge OH oxidation	-4	-2	-2	.	.	.	.	.	.	2
S11	Armchair O_2 oxidation	-2	.	-1	.	+1	.	.	.	.	2
S12	Armchair OH oxidation	-2	.	-1	.	+1	.	.	.	.	2

[a] Surface area is updated according to the surface-volume model of Patterson and Kraft [29].
[b] Increment number of uniformly chosen sites according to table 3(a).
[c] Decrement number of uniformly chosen sites according to table 3(b).

Table 3: *Particle state changes when incrementing sites. Reverse signs for decrementing changes.*

(a) Site Incrementing

Original Site	N_{ed}	N_{zz}	N_{ac}	N_{bay}	N_{R5}
Free-edge	-1	+1	.	.	.
Zig-zag	.	-1	+1	.	.
Armchair	.	.	-1	+1	.
Hole	.	.	.	-1	.

(b) Site Decrementing

Original Site	N_{ed}	N_{zz}	N_{ac}	N_{bay}	N_{R5}
Zig-zag	+1	-1	.	.	.
Armchair	.	+1	-1	.	.
Hole	.	.	+1	-1	.

study was conducted using the KMC code [8]. For each process the current state of the PAH molecule, as it applies in the site counting model, was stored. The neighbours of the site selected for reaction were noted. The code was run several times at different temperature and for different molecules, to provide a large data set of reaction events and the corresponding neighbouring sites. This allowed the probability distribution of the neighbouring sites to be found. The neighbour weight distributions for each process are listed in table 4. Generation of these weights is discussed in a subsequent section.

5 Model validation

Development of the correlations for combined sites and the probabilities of sites acting as neighbours, which are required by the site-counting model, is detailed here. Additionally, the effect of steric hinderance in larger PAH structures is investigated.

5.1 Combined-Site Correlations

As explained above, the site-counting model requires information about the PAH structures in the form of correlations and statistics. Figure 4 shows two combined sites on a PAH structure computed using the KMC-ARS model. The correlations for the combined sites were based on the variation in their counts with the count of one of their constituent elementary sites. To obtain the correlations, the simulation of the growth of PAH molecules was carried out 50 times and the combined site counts were stored along with the elementary site counts. Figure 5 shows an average variation in the number of two combined sites with the number of elementary sites. A nearly linear relationship was observed in all cases. A least-squares algorithm was used to fit a linear function to the data, averaged over all simulations, to obtain the correlations.

The correlations for all the combined sites required by the site-counting model are given below:

Table 4: *Neighbouring site probability weight distributions for each stochastic process.*

Process		**Site**	$\mathbf{P}_{ed}$	$\mathbf{P}_{zz}$	$\mathbf{P}_{ac}$	$\mathbf{P}_{bay}$
S1	Free-edge growth	Free-edge	0.10	0.27	0.40	0.23
S2	Free-edge desorption	R6	0.00	0.05	0.61	0.34
S3	R5 addition	Zig-zag	N/A			
S4	R5 desorption	R5	N/A			
S5	Armchair growth	Armchair	0.68	0.20	0.04	0.08
S6	R5 free-edge conversion	ED-R5	0.25	0.25	0.25	0.25
S7	R5 free-edge desorption	AC-R6	0.00	0.06	0.57	0.37
S8	R5 armchair conversion	AC-R5	0.25	0.25	0.25	0.25
S9	O_2 free-edge oxidation	R6	0.00	0.32	0.39	0.29
S10	OH free-edge oxidation	R6	0.00	0.36	0.41	0.23
S11	O_2 armchair oxidation	Armchair	0.00	0.08	0.53	0.39
S12	OH armchair oxidation	Armchair	0.00	0.08	0.38	0.54

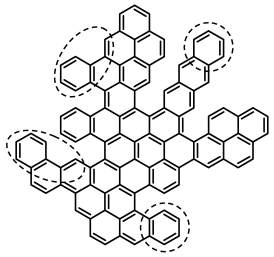

Figure 4: *A computed PAH molecule after a simulation time of 0.1 ms. The combined sites involving three adjacent free-edges (R6 ring) are shown inside circles. The combined sites involving an R6 ring next to an armchair (R6_AC) are shown inside ellipses.*

$$N_{R6} = \begin{cases} 0.136 \times (N_{FE} - 2) & \text{if } N_{FE} > 2 \\ 0 & \text{if } N_{FE} \leq 2 \end{cases} \tag{3}$$

$$N_{AC\_R6} = \begin{cases} 0.174 \times N_{AC} & \text{if } N_{FE} > 2,\ N_{AC} > 0 \\ 0 & \text{if } N_{FE} \leq 2,\ N_{AC} \leq 0 \end{cases} \tag{4}$$

$$N_{R5FE} = \begin{cases} 1.33 \times N_{R5} & \text{if } N_{FE} > 0,\ N_{R5} > 0 \\ 0 & \text{if } N_{FE} \leq 0,\ N_{R5} \leq 0 \end{cases} \tag{5}$$

$$N_{R5AC} = \begin{cases} 0.1 \times N_{R5} & \text{if } N_{AC} > 0,\ N_{R5} > 0 \\ 0 & \text{if } N_{AC} \leq 0,\ N_{R5} \leq 0 \end{cases} \tag{6}$$

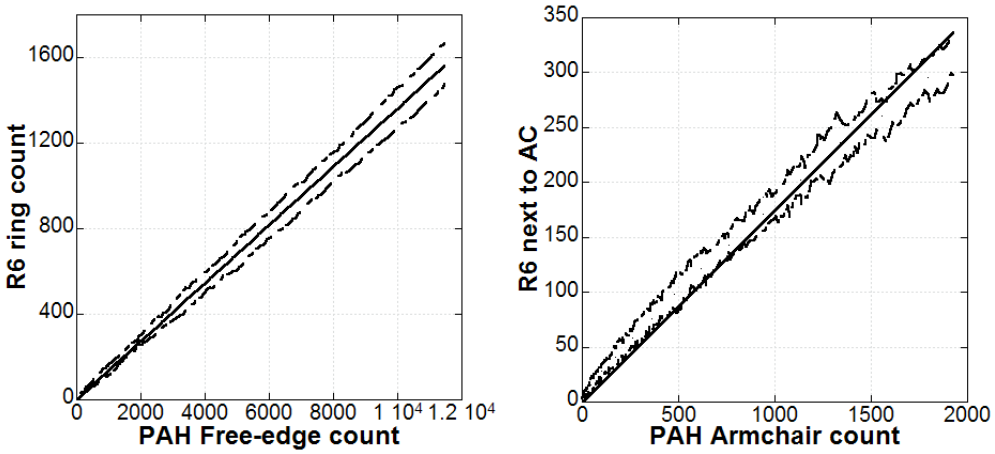

(a) R6 ring count as a function of free-edge count.

(b) AC_R6 site count (R6 ring next to an armchair) as a function of armchair count.

Figure 5: *Correlations for combined sites. Solid lines show linear approximations, dashed lines show confidence intervals. Confidence interval is an estimate of the statistical fluctuation of a variable [8].*

5.2 Neighbour Statistics

A PAH process on a site affects at least two other neighbouring sites. Therefore, after every reaction, it is necessary to update the neighbouring sites. In the site-counting model, the neighbouring sites for each reaction are determined using the probability of occurrence of a site as a neighbour in a reaction. Only processes 1,2,5,7 and 9–12 in table 1 are considered here, as those involving only 5-member rings do not change neighbouring sites, and processes 7 and 8 were observed to occur so infrequently that meaningful statistics could not be obtained. It was initially assumed that neighbouring sites of type $S \in \{ED, ZZ, AC, BY\}$ are selected for process m with the probability $P_{S,k}(m) = N_{S,k}/N_{tot,k}$, where $N_{S,k}$ is the number of sites of type S at time k, $N_{tot,k}$ is the total number of sites (ignoring 5-member rings), and $m \in \{1, 2, 5, 7, 9, \ldots, 12\}$ is the process index (see table 1). However, it was found that when using these probabilities the site-counting model did not agree with the KMC-ARS model, which suggests that some sites are more likely than others to be neighbours for certain processes. Therefore, site count weights were introduced for each process such that the weighted counts are given by: $N'_{S,k} = W_{S,k}(m) \times N_{S,k}$, hence the probability of a site of type S being selected at time k for process m becomes:

$$P_{S,k}(m) = \frac{N'_{S,k}(m)}{N'_{tot,k}(m)} \tag{7}$$

where $N'_{tot,k}(m)$ is the sum of the weighted site counts and depends on the process m. It is assumed that the site weights do not depend strongly on PAH size, therefore they are considered to be constant for each process. This assumption is supported by the KMC-

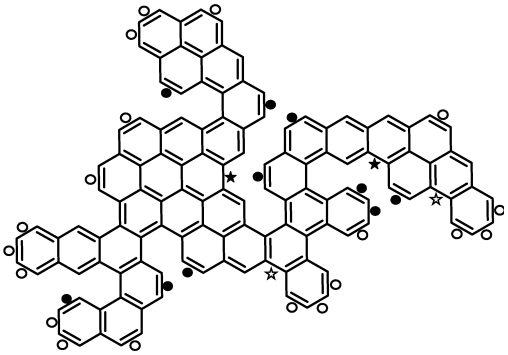

Figure 6: *A computed PAH molecule formed after 0.1 ms. Filled circles and stars denote unavailable free-edges and armchairs respectively. Hollow symbols denote available sites. 2 out of 4 armchairs and 10 out of 29 free-edges are unavailable.*

ARS simulations conducted for this study.

In order to calculate the site weights, several KMC-ARS simulations were performed. For each simulation there are K events, and K_m denotes the number of times event m occurred. On selection of the k^{th} jump process, where $k = 1, 2, \ldots, K$, the following information was stored: the time point k, the jump process index, m_k, the types of both neighbour sites, $T_{1,k}$ and $T_{2,k}$ and the counts of all site types; $N_{ED,k}$, $N_{ZZ,k}$, $N_{AC,k}$, $N_{bay,k}$. $L_{S,m}$ shall denote the number of times a site of type S acted as a neighbour for process m. In the limit of large K_m, the probability of a site acting as a neighbour is assumed to approach $P_S(m) = L_{S,m,k}/K_{m,k}$, therefore, by summing over each jump process and solving the following equation, the site weights can be obtained:

$$\sum_{k=1}^{K_m} \frac{W_S N_{S,k}}{W_{FE} N_{FE,k} + W_{ZZ} N_{ZZ,k} + W_{AC} N_{AC,k} + W_{bay} N_{bay,k}} = L_{S,m} \tag{8}$$

where $S \in \{ED, ZZ, AC, BY\}$ and $m \in \{1, 2, 5, 7, 9, \ldots, 12\}$. As there are four possible site types which may act as neighbours; free-edges (FE), zig-zags (ZZ), armchairs (AC) and bays, equation 8 gives a system of eight linear equations, which can be solved using a standard numerical technique such as a Newton method. Equation 8 was solved for the four elementary sites, with the additional constraints of $W_S \geq 0$ and $\sum_S W_S = 1$. Table 4 shows the site-probabilities for the principal reactions.

5.3 Unavailable Sites

As a PAH molecule grows, some of the reactive sites become hindered due to the presence of neighbouring sites. Figure 6 shows the presence of unavailable free-edges and armchairs on a computed PAH molecule. Further growth on those reactive sites is possible only if the PAH molecule is allowed to adopt a 3D structure due to the interaction between nearby H atoms. However, in a stack, due to the presence of nearby PAHs, 3D geometry

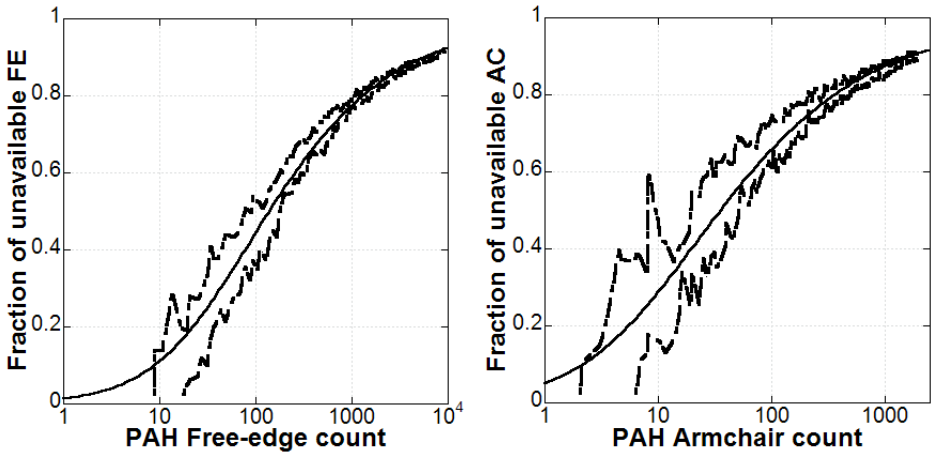

(a) Fraction of unavailable free-edges. (b) Fraction of unavailable armchairs.

Figure 7: *Unavailable sites. Solid lines show a* tanh *fit. Dashed lines show the confidence intervals.*

of a PAH may not be possible. It is most likely that the H atoms are abstracted and a six-member ring is formed through cyclo-dehydrogenation processes. These processes have been ignored in this study, and their influence is highlighted as work requiring further study.

It is possible to determine the number of unavailable sites using the KMC-ARS model. Figures 7(a) and 7(b) show the fraction of unavailable free-edges and armchairs respectively as functions of the free-edge and armchair counts. These fractions firstly increase with the site counts and then attains an asymptotic limit of about 0.9 at larger site counts. A function of the form $Y = \tanh(a \times \log(bX + 1))$ was found to describe this asymptotic behaviour well. The curves in figure 7 were fitted by trial and error, and the equations are given below:

$$N_{unavail'FE} = \tanh(0.593 \times \log(0.054 \times N_{FE} + 1) \quad (9)$$

$$N_{unavail'AC} = \tanh(0.571 \times \log(0.23 \times N_{AC} + 1) \quad (10)$$

5.4 Validation

To validate the site-counting model, the correlations and statistics described above were implemented in the site-counting model, and identical simulations were performed using the two models. The simulation parameters are given in table 5.

Figure 8 shows the comparison of the PAH characteristics: carbon atom count and number of elementary sites on the PAH. Figure 8(a) shows that the site-counting model and the KMC-ARS model predict similar carbon atom counts at all observed flow times. Figure 8(b) shows that the agreement for the number of free-edges, zig-zags and armchairs

Table 5: *Simulation parameters for PAH growth validation simulations.*

Parameters	Initial value
Temperature	1650 K
Pressure	1 atm
$X_{C_2H_2}$	10^{-1}
X_{H_2}	10^{-1}
X_H	10^{-2}
X_{OH}	10^{-4}
X_{O_2}	10^{-2}
Starting structure	Pyrene ($C_{16}H_{10}$)
Free edges	6
Zigzags	4
Residence time, t_{stop}	2.4 ms

is reasonable also. The close agreement of the number of elementary sites is important because the site counts are used to calculate the process rates. The extent of agreement of the computed PAH characteristics by the two models is very encouraging. These comparisons provide an adequate ground for the implementation of the site-counting model into a soot particle population balance.

As the PAH molecules present in flames are very small in size (PAHs with less than 100 C atoms are observed in flames [10, 32]), a comparison between the two models was carried out over this range with and without the correlation for unavailable sites, to test its importance in the experimental size range. Figure 9 shows the variation in the number of PAH sites with the number of C atoms for this case. It can be concluded from this figure that the correlations for unavailable sites are not very significant for small PAH molecules.

6 Particle structure model

While 2D surface-volume models, such as that described by Patterson and Kraft [29], can provide an estimation of the aggregation structure of soot particles, they are limited by the restrictive assumptions made. An estimate average primary particle size can be calculated, although in reality there will be a distribution of primary-particle sizes within an aggregate. High-precision 3D models [4, 25] are able to describe the aggregation structure of soot particles completely, but are very computationally expensive. Recently a simple primary-particle model has been developed [36], originally for titania nanoparticles, though the model also applies to sooting systems. The model is essentially an extension of the surface-volume model, in that it uses the volume and surface area prediction of that model to inform a list of spherical primary particles. This list is stored independently of the surface-volume parameters for each particle. In this extension to the model, the sizes of the primary particles within each agglomerate particle are also tracked, hence the minimum particle state space becomes $E_{pp} = (C, S, p)$, where $p = (p_1, p_2, p_3, \ldots)$

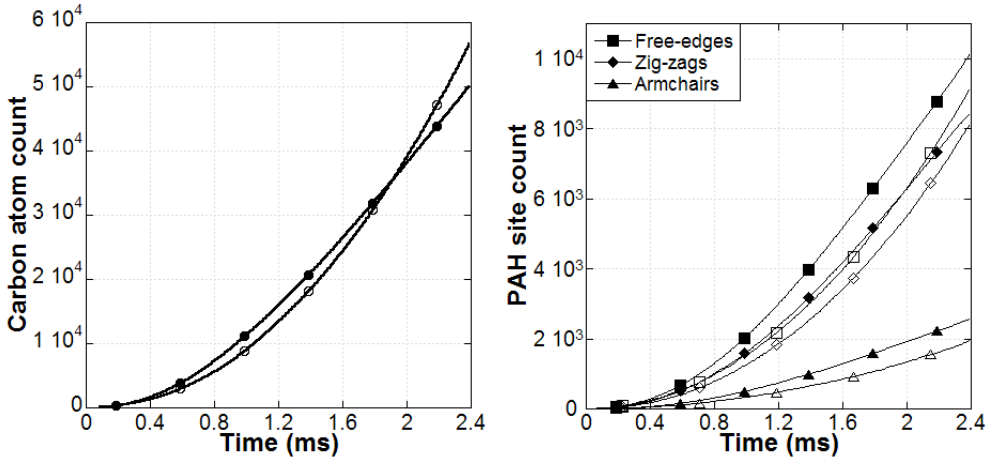

(a) C atom count as a function of time

(b) Site count as a function of time

Figure 8: *Comparison of the results from the KMC-ARS model and the site-counting model. Filled symbols show the results from the site-counting model and hollow symbols show the result from the KMC-ARS model.*

is the vector of primary particle masses. For a simulation in which the highest number of primaries in a single agglomerate reaches N, the population balance effectively has $(N + 2 - 1)$ dimensions. When combined with the site-counting model, the complete state space of the computation particles is

$$E_{scpp} = (C, H, N_{ed}, N_{zz}, N_{ac}, N_{bay}, N_{R5}, S_a, N_{PAH}, p)$$

which has $(N + 8)$ dimensions. This is the particle description used for subsequent simulations.

On inception a computation particle is assigned a single primary, with the same mass as the particle. On coagulation the primary particle lists of the two aggregates are combined. The lists are stored in order of primary size for computational efficiency, and this order is maintained when the lists are combined. Surface growth processes are modelled as follows. According to the surface-volume model [29] all surface processes (growth and oxidation) cause particles to become rounder. This assumption is based on the TEM observation of soot particles. The sintering process, by its nature, also causes an increase of sphericity. The first step of surface growth/oxidation is to add or remove the required mass from the primary particles. As the mass is discretised as the number of carbon atoms, this simply involves adding/removing a set number of C atoms from the list. Atoms are added/removed randomly from primaries weighted by their surface area using a binomial process. A similar algorithm is used to describe particle rounding by any process. Rounding in general reduces the number of primary particles in the aggregate, and the primaries get larger. This is modelled by removing primaries, starting with the smallest, and distributing that mass over the remaining primaries in an identical manner as surface growth. This procedure is repeated until the surface area of the primary particles is less than or

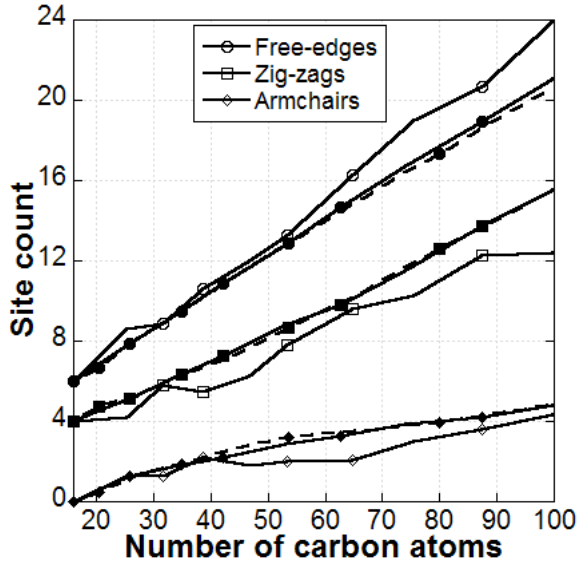

Figure 9: *Comparison of the results: Filled symbols show the results from the site-counting model and hollow symbols from the KMC-ARS model. Dashed lines show the results from site-counting model without correlations for unavailable sites.*

equal to the predicted by the surface-volume model. This is shown schematically in figure 10.

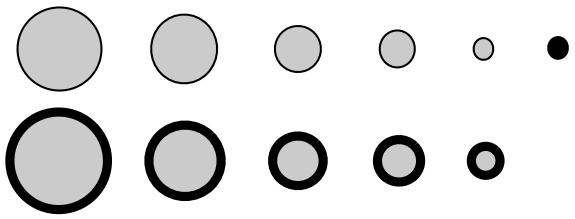

Figure 10: *Primary particles before (top) and after (bottom) surface growth rounding.*

The combined soot particle model incorporating the ARS site-counting model and the primary-particle description has been integrated into the in-house stochastic particle solver SWEEP. This code is available upon request.

6.1 TEM-style image generation

In the models described so far no structural information about an aggregate, such as the position of the primary particles with respect to each other, is taken into account and hence is not available in an implementation. Nonetheless there exist several ways of deducing at least approximations to probable shapes of aggregates, for example diffusion limited cluster-cluster aggregation (DLCA) [20, 24], valid in the continuum regime, and

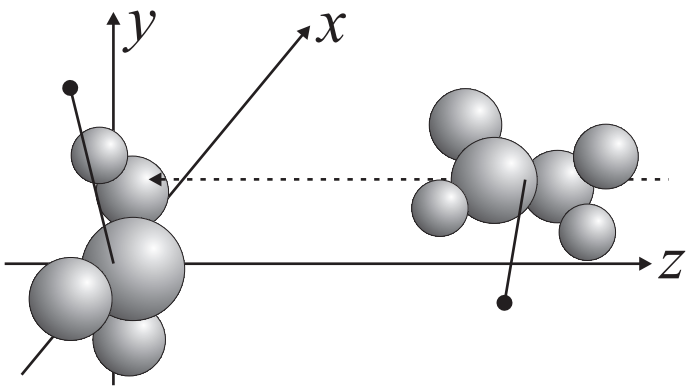

Figure 11: *Schematic of ballistic aggregation of two clusters of primary particles.*

ballistic cluster-cluster aggregation (BCA) [19], valid in the free-molecular regime. Since these models are generally applied to systems in the free molecular regime, only BCA is considered here. However, for large aggregates formed in Diesel engines for example, BCA is not applicable since aggregation is diffusion limited in this case.

One of the simplest ways of generating an aggregate geometry is by imitating the physical history the aggregate goes through. In algorithmic language:

1. Create a list of aggregates where each aggregate is initialized as containing only a single primary particle of the original aggregate. In other words the list corresponds to the list of primary particles of the original aggregate.
2. Pick two distinct aggregates from the list randomly with uniform distribution.
3. Collide the two aggregates as described below, delete one of the picked aggregates and replace the other one with the collided one.
4. If there is more than one aggregate left in the list, go to step 2.

The collision of two aggregates is carried out as follows:

1. Place the first aggregate such that its center of mass is at the origin, and rotate it to a uniformly random orientation.
2. Place the second aggregate such that its center of mass lies on the positive z-axis sufficiently distant from the origin so that it does not touch or intersect the first aggregate, and rotate it to a uniformly random orientation.
3. Translate the second aggregate within the x-y-plane by not more than the sum of the radii of the two aggregates.
4. Test collision if the second aggregate were moved along the z-axis towards the origin.
5. If there is no contact at all, go to step 2.

This algorithm is illustrated in Fig. 11.

For small aggregates, testing the collision between every sphere (primary particle) in aggregate 1 with every sphere in aggregate 2 is computationally feasible. However, there exist much more efficient algorithms for collision testing of complex objects, developed by the video game programming community. Colliding two spheres is a simple exercise in elementary geometry.

Step 4 assumes free motion along a linear trajectory, which is valid in the free molecular regime.

A typical example for a structure resulting from the above algorithm, rendered with the POV-Ray ray tracing software, is given in Fig. 15(a).

7 Premixed flame simulation

The premixed flame C4 of Abid et al. [1] have been simulated used the model detailed here, as experimentally obtained data were available for many properties of interest. The premixed flame chemistry was solved using the PREMIX code [22], including a method-of-moments approximation for soot formation [12]. The Monte-Carlo particle solver (SWEEP) was then run as a post-processing step [6] using the ARS-SC-PP model. An improved O_2 oxidation rate, detailed by Celnik et al. [7], has been incorporated into the ARS chemistry and used for these simulations.

Fig. 12 shows the comparison of the ARS-SC-PP model to the experimentally observed soot volume fraction (Fv). There is a broad agreement between the simulations and the experiments, in particular when considering the confidence intervals due to the uncertainty in the measured temperature profiles. There is a difference between the soot density of 1.5 g/cm^3 assumed by Abid et al. and the value of 1.8 g/cm^3 used here, which might account for the small discrepancy between the simulations and the experiments.

Fig. 13 shows the comparison of the ARS-SC-PP model to the experimentally obtained particle size distribution (PSD) at a height above burner of 1.0 cm. The PSDs were calculated using the kernel density estimation (density) function of the statistical package R [16] with a bandwidth of $0.03 \times d$, where d is the aggregate collision diameter [29]. The simulation demonstrates a reasonable fit to the experimental data. At the first HAB = 0.5 cm the simulation already predicts bimodality, which is not observed in the experimental data, however, there is a severe underprediction of the largest particles' concentrations, although the trough at around 4-4.5 nm almost match the experimental data. The bimodal nature of the experimental data is well predicted. The disagreement at larger particle sizes is possibly indicative of a coagulation effect.

Fig. 14 shows the particle C/H ratio distribution against particle diameter at HAB = 1.0 cm. The 2D kernel density estimation (kde2d) function of R was used to calculate the distribution, using 100 points in each direction. The bimodality of the particle distribution can be clearly seen. The left-most density maximum occurs around C/H = 1.6, which is equivalent to pyrene ($C_{16}H_{10}$). This is an artefact of the soot inception model used, which assumes that the dimerisation of pyrene is the only route of particle formation, so in this

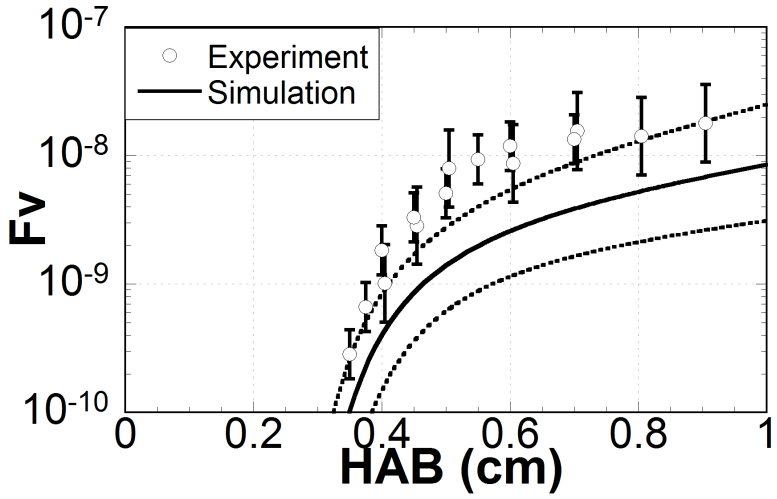

Figure 12: *Soot volume fraction as a function of height above burner. Short-dashed lines indicate confidence intervals due to the 50 K uncertainty in the experimentally measured flame temperature. HAB shifted by +0.15 cm.*

respect the result is uninteresting. The second peak occurs at C/H values around 2, which is consistent with reported values for young soot particles [33]. It is interesting that there is little variation of the C/H ratio for particles between 10-40 nm, in fact the C/H ratio appears to converge on a value just below 2. Far higher ratios are presented in the literature, for example Harris & Weiner [17] report about 7 and Homann [18] reports about 10. It has been suggested [9] that a process such as graphitisation could be responsible for such an increase in C/H ratio, but this has not been considered here.

8 Engine soot modelling

The detailed soot models outlined in the previous sections have also been applied to soot formation in internal combustion engines. To this end, the SWEEP library has been implemented into the in-house engine model, called the Stochastic Reactor Model (SRM). The SRM is inspired by Probability Density Function (PDF) transport methods [30] and has been successfully employed in a number of earlier engine studies without taking soot into account, for example [26, 27]. The main features of this model include detailed chemical kinetics, and a statistical representation of inhomogeneities in the in-cylinder gases, that is of stratification in composition as well as temperature. A key advantage compared to other approaches is that this model is computationally cheap with about one to two hours of CPU-time per engine cycle, enabling convenient multi-cycle and sensitivity studies.

As a fuel model a detailed chemical mechanism for Primary Reference Fuels (PRFs, n-heptane/iso-octane mixtures) containing 208 species and 1002 reactions is used, which has been extended [28] to include small PAHs such as pyrene which function as inception species as described in previous sections.

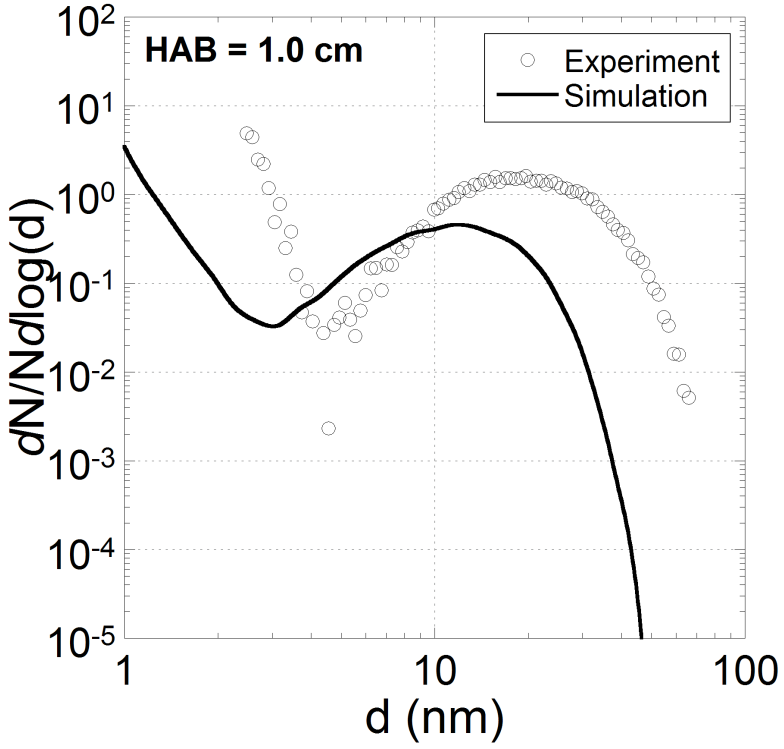

Figure 13: *Particle size distribution at different a height above burner of 1.0 cm (shifted by +0.15 cm).*

In a first attempt to model soot formation in detail in an engine, a Homogeneous Charge Compression Ignition (HCCI) engine is chosen, that is an engine in which fuel (here pure n-heptane) and air are fully premixed, and (auto-)ignition is triggered simply through compression. Since the aim is to study soot formation, an equivalence ratio of 1.93 was chosen. In order to operate an engine so rich, high levels of Exhaust Gas Recirculation (EGR) are required, that is significant amounts of burnt gases - including particulate matter such as soot if present - are fed back into the next engine cycle.

Figure 15 shows a typical simulated aggregate rendered in TEM-style (Fig. 15(a)) together with its size distribution of primary particles (Fig. 15(b)). It was sampled from the engine cylinder at 48.2 crank angle degrees (CAD) after top dead centre (ATDC) and possesses a collision diameter of about 77.8 nm.

In Fig. 16, simulated in-cylinder aggregate size distributions at 11 CAD ATDC are shown for eight consecutive cycles. It is observed that the distributions converge quickly across the entire size range as the cycle number increases, and also that aggregates larger than in this case about 30 nm stem almost exclusively from previous cycles. From this it is concluded that, with high likelihood, parts of the aggregate in Fig. 15(a) have been recirculated at least once.

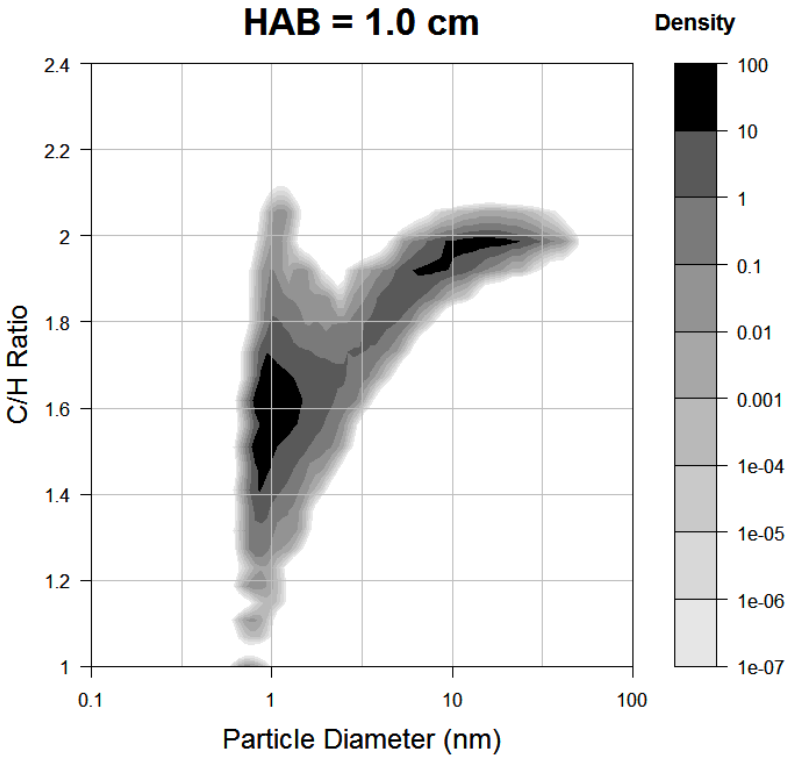

Figure 14: *Particle C/H Ratio density plot against particle diameter at HAB = 1.0 cm.*

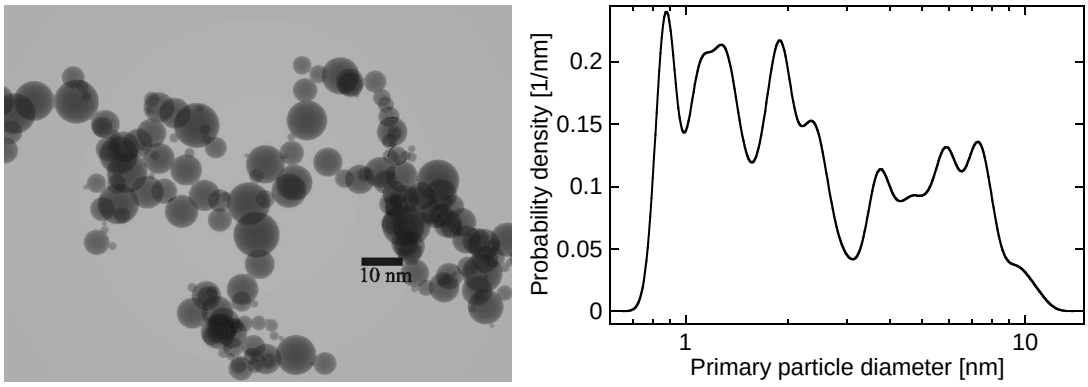

(a) TEM-style image of aggregate (223 primaries, collision diameter 77.8 nm).

(b) Primary particle size distribution of aggregate 15(a).

Figure 15: *Typical simulated aggregate sampled at 48.2 CAD ATDC, with size distribution of primary particles.*

9 Conclusions

In this article an overview of the multivariate soot particle model ARS-SC-PP has been presented. A discussion of a method of incorporating soot chemical structure into the particle model has been discussed in the context of the site-counting model. The site-counting model has been presented as an efficient method of tracking detailed soot chemical structure, but still allowing particle ensembles to be simulated in reasonable computation times. Validation and term closure of the site-counting model has been performed by using a 2D kinetic-Monte Carlo technique. A discussion of a primary-particle structure model, which has a complexity and speed advantage in between those of the surface-volume models and the full 3D aggregate models has been reviewed. The generation of an approximate 3D particle structure from this model has been presented, which allows representative TEM-style images to be generated for sooting systems. This is a very useful diagnostic tool. The soot model has been used to simulate a premixed flame, and the predictions were compared to the experimental results. Finally an application of this advanced soot model has been presented, by incorporating the model into a stochastic reactor model for internal combustion engines. The computational efficiency and detailed chemical and structural information available from these models make them very useful for the characterisation of such complex systems.

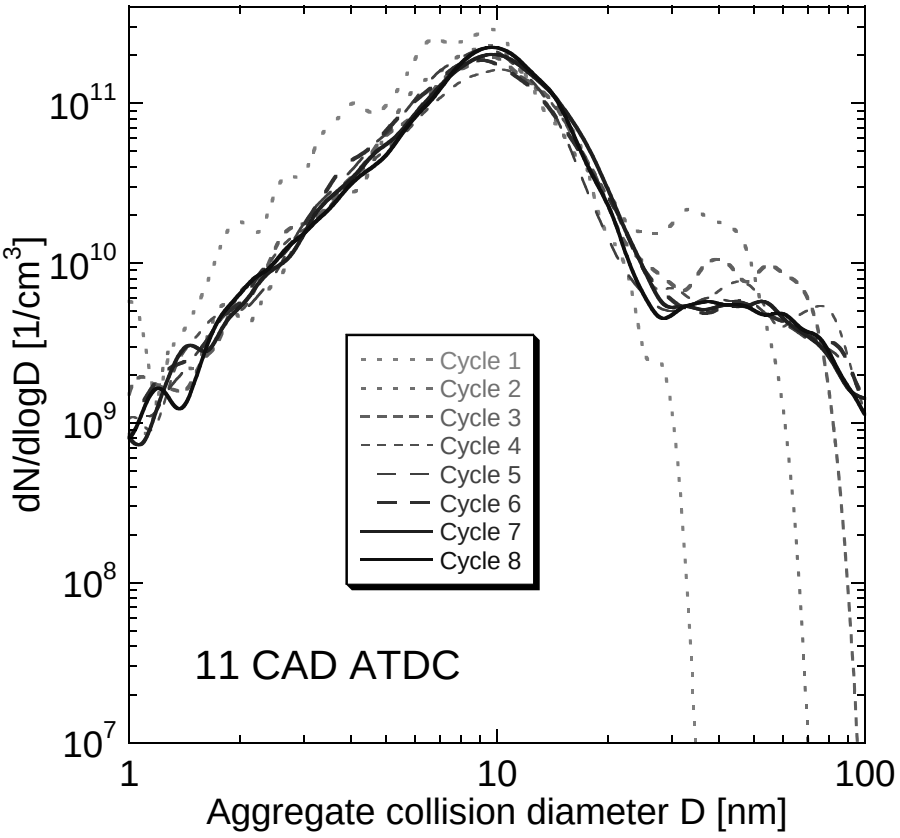

Figure 16: *Simulated in-cylinder aggregate size distribution functions at 11 CAD ATDC for eight consecutive cycles. The distributions stabilize across the whole size range after the first few cycles, whilst revealing the role of the recirculated aggregates with sizes above about 30 nm.*

References

[1] A. D. Abid, N. Heinz, E. D. Tolmachoff, D. J. Phares, C. S. Campbell, and H. Wang. On the evolution of particle size distribution functions of soot in premixed ethylene-oxygen-argon flames. *Combust. Flame*, page submitted, 2007.

[2] J. Appel, H. Bockhorn, and M. Frenklach. Kinetic modeling of soot formation with detailed chemistry and physics: Laminar premixed flames of C_2 hydrocarbons. *Combust. Flame*, 121:122–136, 2000. doi:10.1016/S0010-2180(99)00135-2.

[3] J. Appel, H. Bockhorn, and M. Wulkow. A detailed numerical study of the evolution of soot particle size distributions in laminar premixed flames. *Chemosphere*, 42: 635–645, 2001. doi:10.1016/S0045-6535(00)00237-X.

[4] M. Balthasar and M. Frenklach. Detailed kinetic modeling of soot aggregate formation in laminar premixed flames. *Combust. Flame*, 140:130–145, 2005.

[5] M. Balthasar and M. Frenklach. Monte-Carlo simulation of soot particle coagulation and aggregation: The effect of a realistic size distribution. *Proc. Combust. Inst.*, 30: 1467–1475, 2005. doi:10.1016/j.proci.2004.07.035.

[6] M. Balthasar and M. Kraft. A stochastic approach to solve the particle size distribution function of soot particles in laminar premixed flames. *Combust. Flame*, 133: 289–298, 2003. doi:10.1016/S0010-2180(03)00003-8.

[7] M. S. Celnik, A. Raj, R. I. A. Patterson, R. H. West, and M. Kraft. A statistical approach to develop a detailed soot growth model using PAH characteristics. Technical Report 53, c4e Preprint-Series, Cambridge, 2007. URL `http://como.cheng.cam.ac.uk`.

[8] M. S. Celnik, M. Sander, A. Raj, R. H. West, and M. Kraft. Modelling soot formation in a premixed flame using an aromatic-site soot model and an improved oxidation rate. Technical Report 52, c4e Preprint-Series, Cambridge, 2007. URL `http://como.cheng.cam.ac.uk`.

[9] M. S. Celnik, A. Raj, R. H. West, R. I. A. Patterson, and M. Kraft. An aromatic site description of soot particles. *Combust. Flame*, page in press, 2008. doi:doi:10.1016/j.combustflame.2008.04.011.

[10] H. X. Chen and R. A. Dobbins. Crystallogenesis of Particles Formed in Hydrocarbon Combustion. *Combust. Sci. Technol.*, 159:109–128, 2000.

[11] M. Frenklach. On surface growth mechanism of soot particles. *Proc. Combust. Inst.*, 26:2285–2293, 1996. doi:10.1016/S0082-0784(96)80056-7.

[12] M. Frenklach. Method of moments with interpolative closure. *Chem. Eng. Sci*, 57: 2229–2239, 2002. doi:10.1016/S0009-2509(02)00113-6.

[13] M. Frenklach and J. Ping. On the role of surface migration in the growth and structure of graphene layers. *Carbon*, 42:1209–1212, 2004. doi:10.1016/j.carbon.2004.01.025.

[14] M. Frenklach and H. Wang. Detailed modeling of soot particle nucleation and growth. *Proc. Combust. Inst.*, 23:1559–1566, 1990. doi:10.1016/S0082-0784(06)80426-1.

[15] M. Frenklach, C. A. Schuetz, and J. Ping. Migration mechanism of aromatic-edge growth. *Proc. Combust. Inst.*, 30:1389–1396, 2005. doi:10.1016/j.proci.2004.07.048.

[16] R. Gentleman and R. Ihaka. R statistical software, 2005. URL `www.r-project.org`. version 2.4.0.

[17] S. J. Harris and A. M. Weiner. Chemical kinetics of soot particle growth. *Ann. Rev. Phys. Chem.*, 36:31–52, 1985. doi:10.1146/annurev.pc.36.100185.000335.

[18] K. H. Homann. Carbon formation in premixed flames. *Combust. Flame*, 11(4): 265–287, 1967. doi:10.1016/0010-2180(67)90017-X.

[19] R. Jullien. Transparency effects in cluster-cluster aggregation with linear trajectories. *Journal of Physics A: Mathematical and General*, 17:L771–L776, 1984. doi:10.1088/0305-4470/17/14/009.

[20] R. Jullien, R. Botet, and P. M. Mors. Computer simulations of cluster-cluster aggregation. *Faraday Discussions of the Chemical Society*, 83:125–137, 1987. doi:10.1039/DC9878300125.

[21] A. Kazakov and M. Frenklach. Dynamic modeling of soot particle coagulation and aggregation: Implementation with the method of moments and application to high-pressure laminar premixed flames. *Combust. Flame*, 114:484–501, 1998. doi:10.1016/S0010-2180(97)00322-2.

[22] J. Kee, K. Grcar, M. D. Smooke, and J. A. Miller. Premix: A fortran program for modelling steady laminar one-dimensional premixed flames. Technical report, SANDIA National Laboratories, 1985.

[23] U. O. Köylü. Quantitative Analysis of In Situ Optical Diagnostics for Inferring Particle/Aggregate Parameters in Flames: Implications for Soot Surface Growth and Total Emissivity. *Combust. Flame.*, 109:488–500, 1996. doi:10.1016/S0010-2180(96)00179-4.

[24] P. Meakin. Formation of fractal clusters and networks by irreversible diffusion-limited aggregation. *Physical Review Letters*, 51(13):1119–1122, 1983. doi:10.1103/PhysRevLett.51.1119.

[25] N. Morgan, M. Kraft, M. Balthasar, D. Wong, M. Frenklach, and P. Mitchell. Numerical simulations of soot aggregation in premixed laminar flames. *Proc. Combust. Inst.*, 31:693–700, 2007. doi:10.1016/j.proci.2006.08.021.

[26] S. Mosbach, H. Su, M. Kraft, A. Bhave, F. Mauss, Z. Wang, and J.-X. Wang. Dual injection HCCI engine simulation using a stochastic reactor model. *International Journal of Engine Research*, 8(1):41–50, 2007. doi:10.1243/14680874JER01806.

[27] S. Mosbach, A. M. Aldawood, and M. Kraft. Real-time evaluation of a detailed chemistry HCCI engine model using a tabulation technique. to appear in *Combustion Science and Technology*, 2008.

[28] S. Mosbach, M. S. Celnik, A. Raj, M. Kraft, H. R. Zhang, S. Kubo, and K.-O. Kim. Towards a detailed soot model for internal combustion engines. *in preparation*, 2008.

[29] R. I. A. Patterson and M. Kraft. Models for the aggregate structure of soot particles. *Combust. Flame*, 151:160–172, 2007. doi:10.1016/j.combustflame.2007.04.012.

[30] S. B. Pope. PDF methods for turbulent reactive flows. *Progress in Energy and Combustion Science*, 11:119–192, 1985. doi:10.1016/0360-1285(85)90002-4.

[31] H. Richter, S. Granata, W. H. Green, and J. B. Howard. Detailed modelling of PAH and soot formation in a laminar premixed benzene/oxygen/argon low-pressure flame. *Proc. Combust. Inst.*, 30:1397–1405, 2005. doi:10.1016/j.proci.2004.08.088.

[32] R. L. Vander Wal. An Illustration of Soot Structure by Dark Field Transmission Electrom Microscopy. *Combust. Sci. Tech.*, 132:315–323, 1998.

[33] A. Violi. Modeling of soot particle inception in aromatic and aliphatic premixed flames. *Combust. Flame*, 139:279–287, 2004. doi:10.1016/j.combustflame.2004.08.013.

[34] A. Violi and S. Izvekov. Soot primary particle formulation from multiscale coarse-grained molecular dynamics simulation. *Proc. Combust. Inst.*, 31:529–537, 2007. doi:10.1016/j.proci.2006.07.240.

[35] J. Z. Wen, M. J. Thomson, S. H. Park, S. N. Rogak, and M. F. Lightstone. Study of soot growth in a plug flow reactor using a moving sectional model. *Proc. Combust. Inst.*, 30(1):1477–1484, 2005. doi:10.1016/j.proci.2004.08.178.

[36] R. H. West, M. S. Celnik, O. R. Inderwildi, M. Kraft, G. J. O. Beran, and W. H. Green. Towards a comprehensive model of the synthesis of TiO_2 particles from $TiCl_4$. *Ind. Eng. Chem. Res.*, 46(19):6147–6156, 2007. doi:10.1021/ie0706414.